Imaging Property of a Gas Lens

Y. AOKI, MEMBER, IEEE, AND M. SUZUKI, SENIOR MEMBER, IEEE

Abstract—**Theoretical and experimental analyses on the imaging properties of gas lenses have been performed. The ray trajectory, ray matrix, lens formula, and optical transfer function of gas lenses are discussed. A gas lens of laminar flow type, using temperature gradients of air, has been made and some experiments on the image formation by the gas lens are conducted. To estimate the lens effect, the line spread functions are measured changing the variables which are concerned with the imaging action of the gas lens. The focal length of the gas lens is obtained from the characteristics of the line spread functions. The space-frequency bandwidth of the gas lens is expressed by the optical transfer functions obtained from the line spread functions and from the images of the Simens-star. Further, a telescope arrangement has been made using a gas lens for an object lens and a concave mirror for an eye lens. Experiments were performed with this telescope.**

I. Introduction

OPTICAL TRANSMISSION becomes an important problem for optical communication with the advance of laser techniques and gas lenses have been proposed as a new type of optical guide [1]–[3]. Since then, numerous investigations of gas lenses [4]–[11] have been made in which focusing and guiding of optical beams, losses, aberrations, efficiencies of gas lenses, and other important problems in optical transmission have been discussed.

It is, however, interesting and useful to study gas lenses from the standpoint of formation or transmission of images [12]. For example, we can expect a gas lens to be a parameter variable unlike a single glass lens. In this paper the imaging properties of gas lenses are discussed theoretically and experimentally. In the experiments investigations are made into the characteristics of the real images formed by gas lenses by changing the variables (temperature, gas velocity, distance, etc.) that affect the imaging action of gas lenses. As for how gas lenses function in terms of optical lenses, the line spread function and the optical transfer function are measured considering gas lenses as optical special filters [13], [14] and the space-frequency bandwidth of gas lenses is examined. The focal length of a gas lens is also obtained from the characteristics of the line spread functions. Further, a Keplerian telescope with a gas lens for an object lens and a concave mirror for an eye lens was constructed as an optical instrument using a gas lens. Some experiments on this telescope are described.

Manuscript received May 23, 1966; revised August 8, 1966.

The authors are with the Department of Electronic Engineering, Hokkaido University, Sappro, Japan.

II. Lens Formula and Optical Transfer Function

A. Lens Formula of Gas Lens

In [8] gas lenses are analyzed by a matrix called a ray matrix. Since this matrix is convenient for the discussion on the imaging properties of gas lenses, we derive the ray matrix of a gas lens and discuss the lens formula and the optical transfer function of gas lenses. The analysis is based on the geometrical optics and the wave vector representation of the eikonal equation which is the fundamental equation in geometrical optics. This is obtained from the Maxwell equations in an approximation $\lambda \to 0, k_0 = (\omega/c) \to \infty$ (λ = wavelength, k_0 = wave number), and is given as follows [15],

$$\text{curl } \boldsymbol{K} = 0 \tag{1}$$

where $\boldsymbol{K}$ is the wave vector of the plane wave and

$$|\boldsymbol{K}| = k = k_0 n = \frac{\omega}{c}\sqrt{\epsilon\mu} \tag{2}$$

where n is the refractive index of the medium. The equation of light rays in arbitrary isotropic media can be obtained from (1).

To simplify the analysis, we consider two-dimensional light rays in a gas lens in which the refractive index varies only along the coordinate x in Fig. 1.

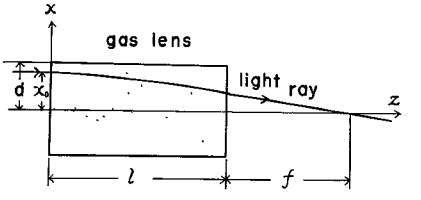

Fig. 1. Gas lens and its focal length. (Refractive index of the gas lens depends only on the coordinate x.)

The characteristic differential equations of (1) are obtained as follows [16], [17],

$$\frac{dx}{k_x} = \frac{dz}{k_z} = \frac{dk_z}{0}. \tag{3}$$

From (3), we obtain the quantity which is conserved along the ray,

$$k_z = \text{constant} = c \tag{4}$$

and with $k_x = \sqrt{k^2 - k_z^2}$ in mind, we can integrate (3) using the relation (4) in the following manner,

$$z = \int^{x} \frac{dx}{\sqrt{\left(\frac{k}{c}\right)^2 - 1}}. \tag{5}$$

Here we take the square-law index variation as an idealized refractive index model in a gas lens that is used in several of the papers referred to, as follows,

$$n = n_0 - n_1\left(\frac{x}{d}\right)^2 \tag{6}$$

where d is the radius of the gas lens and n_1 is a constant concerned with temperature gradients of gas, gas velocity, gas pressure, species of gas, and so forth. Substituting (6) into (5) and integrating with the approximation $n_0 \gg n_1$, we obtain the trajectory of the ray in the gas lens as follows,

$$x = \frac{\alpha}{\beta}\cos\beta(z_0 - z) \tag{7}$$

where

$$\alpha = \sqrt{\left(\frac{k_0 n_0}{c}\right)^2 - 1}, \qquad \beta = \frac{k_0\sqrt{2n_0 n_1}}{cd} \tag{8}$$

$$z_0 = \frac{1}{\beta}\arccos\frac{\beta}{\alpha}x_0 \tag{9}$$

and z_0 is given by the initial condition of the ray. The focal length f of the gas lens as defined in Fig. 1 can be obtained, putting $z_0=0$ in (7) giving the initial condition of parallel rays,

$$f = \frac{1}{\beta}\cot\beta l \tag{10}$$

where l is the length of the gas lens. For paraxial rays, we assume $c=k_z \fallingdotseq k(x=x_0)$ in (8) and take the following approximation,

$$\beta = \frac{\sqrt{2}}{d}\sqrt{\frac{n_1}{n_0}}\left\{1 + \frac{n_1}{n_0}\left(\frac{x_0}{d}\right)^2 + \cdots\right\} \fallingdotseq \frac{\sqrt{2}}{d}\sqrt{\frac{n_1}{n_0}}. \tag{11}$$

Now, we take two variables, the position x and the slope x' of a ray, and the gas lens can be expressed as a linear transformer of x and x' as follows,

$$\begin{bmatrix} x_1 \\ x_1' \end{bmatrix} = \cos\beta l \begin{bmatrix} 1 & \frac{1}{\beta^2 f} \\ -\frac{1}{f} & 1 \end{bmatrix}\begin{bmatrix} x_0 \\ x_0' \end{bmatrix} \tag{12}$$

where the subscripts 0 and 1 denote the variables at the entrance and exit planes of the gas lens, respectively. To simplify the analysis we neglect the refraction on the boundaries between the gas lens and the external space. The matrix of (12) is the same as the matrix derived in [8]. Now, we assume that the image of the object located on the P plane is constructed on the P' plane as shown in Fig. 2. The whole

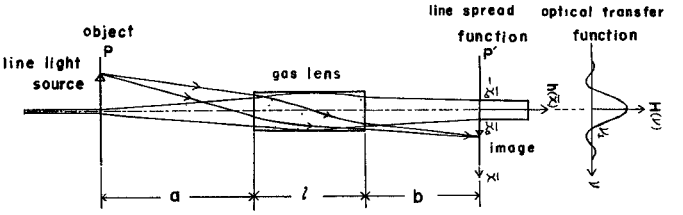

Fig. 2. Image formation and optical transfer function of the gas lens.

matrix that transforms the ray from the P plane to P' plane is obtained by the cascade product of ray matrices of the gas lens and the free spaces as follows,

$$\cos\beta l\begin{bmatrix} 1 & b \\ 0 & 1 \end{bmatrix}\begin{bmatrix} 1 & \frac{1}{\beta^2 f} \\ -\frac{1}{f} & 1 \end{bmatrix}\begin{bmatrix} 1 & a \\ 0 & 1 \end{bmatrix} = \cos\beta l\begin{bmatrix} 1 - \frac{b}{f} & (a+b) - \frac{ab}{f} + \frac{1}{\beta^2 f} \\ -\frac{1}{f} & 1 - \frac{a}{f} \end{bmatrix}. \tag{13}$$

The lens formula of the gas lens can be obtained from the matrix element of (13) as follows,

$$\frac{1}{a} + \frac{1}{b} = \frac{1}{f}\left(1 - \frac{1}{ab\beta^2}\right). \tag{14}$$

If we put $1/ab\beta^2=0$, we get the lens formula of a thin lens.

B. Optical Transfer Function

The optical transfer function (abbreviated as OTF) is frequently used for the estimation of optical systems (e.g., see [18]) where they are considered as optical spatial filters. The OTF is a frequency response of the optical system. The corresponding function is the line spread function (LSF) which is an impulse response of the system. If the line light source is put on the P plane in Fig. 2, then the image of the line light source constructed on the P' plane is the LSF. If we assume that the intensity distribution of the image $h(\bar{x})$ is expressed by a rectangular function with a width $2\bar{x}_0$, we have,

$$\begin{aligned} h(\bar{x}) &= 1 \qquad |\bar{x}| \leqq \bar{x}_0 \\ h(\bar{x}) &= 0 \qquad |\bar{x}| > \bar{x}_0. \end{aligned} \tag{15}$$

Then the OTF $H(\nu)$ of the optical system can be obtained from the Fourier transformation of the LSF of (15),

$$H(\nu) = \int_{-\infty}^{\infty} h(\bar{x}) \exp(-i2\pi\nu\bar{x}) d\bar{x} \propto \frac{\sin 2\pi\bar{x}_0\nu}{2\pi\bar{x}_0\nu} \quad (16)$$

where ν is the space frequency and $\bar{x}$ is the coordinate associated with the image plane P'. From (16), the space frequencies ν_n which give the zero points of $H(\nu)$ are obtained as follows,

$$\nu_n = \frac{n}{2\bar{x}_0}, \qquad n = 1, 2, \cdots. \quad (17)$$

If we neglect the diffraction effect, we can obtain the width $2\bar{x}_0$ of the LSF of the gas lens from the matrix (13) as a two dimensional case. If we assume that the line light source has no width and the ray that gives the boundary $2\bar{x}_0$ of the LSF has the slope x_0' at the source points, we get

$$2\bar{x}_0 = 2x_0' \cos\beta l \left[(a+b) - \frac{ab}{f} + \frac{1}{\beta^2 f}\right], \quad (18)$$

where β depends, in general, on temperature gradients, gas velocity, gas pressure, etc., in such a way that the width $2\bar{x}_0$ depends on these variables and distances a and b. Therefore, if the LSF of the gas lens can be expressed by the rectangular function such as (15), we have only to measure the variation of the width to know how the lens effect of the gas lens varies when the variables concerned with the lens effect are changed.

III. Image Formation by Gas Lens

The gas lenses used in the experiment are laminar flow types and the refractive index gradients are constructed by the temperature gradients of air by setting up a cool air flow through a warmed metal pipe. Figure 3 shows the structure of the gas lens and Fig. 4 is an illustration of the gas lens and the experimental equipment.

The gas lens consists of a metal pipe (brass) with nichrome wire wound around it for warming, and an air source attachment. For insulation, the brass pipe is covered with mica. The electrical current flowing through the nichrome wire is controlled by a slide rheostat and room temperature air is used as the gas. Air is sent through a vinyl tube to the brass pipe by a micro fan (2500 rpm, flow rate 1000 l/min). The wind velocity is controlled by adjusting the air sending attachment. The wall temperature of the metal pipe is measured by a thermometer and the wind velocity at the air outlet of the metal pipe is measured by a hot wire anemometer. As the gas lens used here has a convex lens-like action, the appearance of real images on the ground glass are observed in a dark room in the experimental arrangement shown in Fig. 5, but with the slit replaced by the object shown in Fig. 6(a). The ground glass on which letters and figures are drawn is used as an object and lighted by a projector. The temperature θ_0 is taken as follows,

$\theta_0 = T_w - T_0$

T_w = wall temperature of the metal pipe

T_0 = air input temperature.

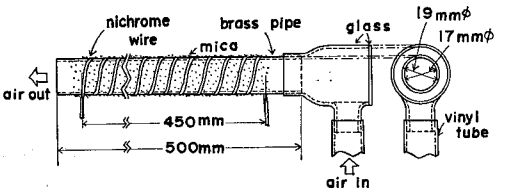

Fig. 3. A gas lens of laminar flow type using the temperature gradients of air.

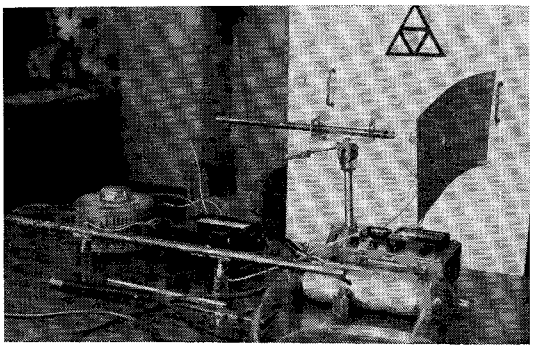

Fig. 4. Photograph of the gas lens shown in Fig. 3 and experimental equipment.

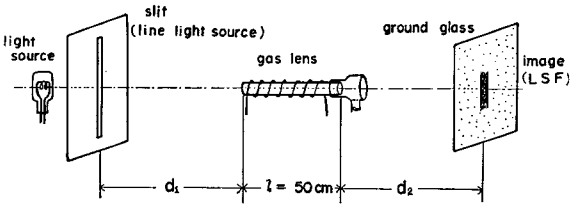

Fig. 5. Experimental arrangement for investigating the imaging property of the gas lens.

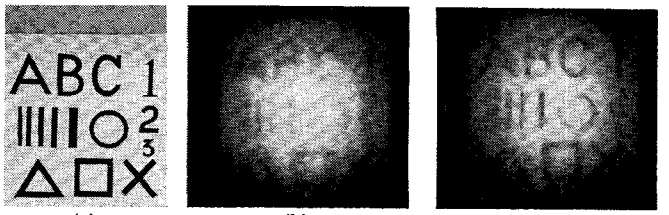

(a) (b) (c)

(a) The object
(b) $\theta_0 = 16°C$
(c) $\theta_0 = 32°C$

Fig. 6. Images of the object (a) formed by the gas lens when the temperature θ_0 is changed. The wind velocity v is 0.25 m/s and the distances are $d_1 = 8.5$ m, $d_2 = 5$ m.

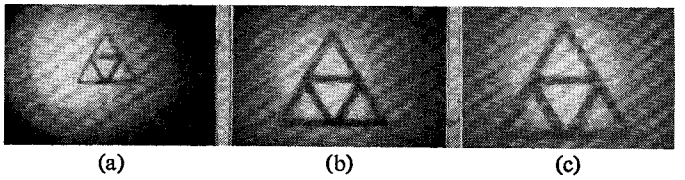

(a) (b) (c)

(a) $d_2 = 4$ m
(b) $d_2 = 8$ m
(c) $d_2 = 10$ m

Fig. 7. Images formed by the gas lens when the distance d_2 between the gas lens and image plane is changed. The temperature θ_0 is 61°C, the wind velocity v is 0.32 m/s and the distance d_1 is 8.8 m.

Figure 6(b) and (c) shows the appearance of the images formed by the gas lens when the temperature θ_0 is changed. The distances shown in Fig. 5 are $d_1=8.5$ m and $d_2=5.0$ m and the wind velocity at the air outlet of the gas lens is $v=0.25$ m/s. Figure 6(b) and (c) corresponds to $\theta_0=16°C$ and 32°C, respectively. In Fig. 6 the photographs show that the lens effect becomes stronger as the temperature θ_0 increases. But when the temperature θ_0 increases to a great extent, the fluctuation of air in the gas lens intensifies, resulting in an intense fluctuation of the images. When the temperature θ_0 is 0°C and the fan is stopped, a very unclear image forms though there should be no imaging action. This is caused by the pin hole effect coming from the small diameter of the metal pipe.

Figure 7(a)–(c) shows the images of the figure seen in Fig. 4 formed by the gas lens when the distance d_2 between the gas lens and the ground glass is changed. Where the temperature θ_0 is 61°C, wind velocity v is 0.32 m/s. and distance d_1 is 8.8 m. From Fig. 7, we see that the images become larger as the distance d_2 increases but the focusing of the images hardly depends on the distance d_2. This is due to the fact that the gas lens in question has a deep focus depth depending on the small diameter of the metal pipe and large focal length.

Further, the appearance of images is observed while the wind velocity is changed from 0 m/s to about 1 m/s and a suitable wind velocity for image formation by the gas lens exists.

IV. Measurement of Line Spread Function

For a more quantitative study of the imaging property of the gas lens, we measure the LSF of the gas lens in the experimental arrangement shown in Fig. 5. The line light source is made by a slit of 1 to 2 mm width which is lighted by a projector. The images of the line light source (LSF) formed by the gas lens are constructed on the ground glass in a dark room and observed. Figure 8 shows the images of the line light source with 2 mm width when the distance d_2 is changed. From Fig. 8 we see that the width of the images becomes narrower as the distance d_2 increases.

Figure 9 shows the images of the line light source with 1 mm width when the temperature θ_0 is changed. From Fig. 9 we see that the width of the images becomes narrower as the temperature θ_0 increases. Figure 9(d) shows, however, that the excessive high temperature causes fluctuation of the image. A double image appears and aberration of the gas lens intensifies. Figures 8 and 9 also show that the intensity distributions of the images of the line light source can be expressed by the rectangular functions as shown (15) within the limits of appropriate temperature and wind velocity. Therefore, we consider the LSF of the gas lens to be a rectangular function with the width $2\bar{x}_0$ and we measure the variation of the width when the variables and parameters (θ_0, v, d_2) are changed.

Figure 10 shows the variation of the LSF when the temperature θ_0 is changed with the wind velocity as a parameter. The width $2x_0$ becomes narrower as the temperature θ_0 increases, because the lens effect of the gas lens becomes stronger. The lens effect also becomes stronger as the parameter of the wind velocity becomes larger, but the larger the wind velocity becomes, the more difficult is it to keep the stable temperature gradients of air. It also becomes difficult to measure the width in the case of excess high temperature and large wind velocity.

Figure 11 shows the variation of the width $2\bar{x}_0$ of the LSF when the wind velocity is changed with the temperature θ_0 as a parameter. Figure 11 shows that the width becomes narrower as the wind velocity increases. However, there is a tendency for the width to become greater as the wind velocity increases from a certain value. This fact is due to the fluctuation of air.

Figure 12 shows the variation of the width $2\bar{x}_0$ when the distance d_2 is changed. From Fig. 12 we see that when the temperature θ_0 is low and the gradients of the temperature are slight the width of the images becomes greater as the distance d_2 increases. This is due to the fact that the focusing effect of the gas lens is not strong enough to make the rays converge. When the temperature becomes high, we see that the images become narrower as the distance d_2 increases because of the strong focusing effect.

V. Measurement of Focal Length

Several of the papers referred to reported on the use of laser light for parallel rays to measure the focal length of gas lenses. In this section we measure the focal length of the gas lens by the characteristics of the LSF. This method is useful when we cannot get parallel rays of good quality though it requires more labor. From Fig. 12, we see that for a certain value of temperature, the widths of the LSF of the gas lens do not depend on the distance d_2. This is analogous to the images of the line light source which are placed at the focus of a convex lens. This suggests a method for obtaining the focal length of the gas lens. That is to say the distance d_1 corresponds to the focal length of the gas lens. Therefore, we define the distance d_1 as the focal length of the gas lens. But the focal length seen from the right side of the gas lens of laminar flow type may be different from that seen from the left side, since the gas flow is unidirectional. The focal length discussed here is that of the left side (side of the object plane) in Fig. 5. Thus, for a fixed value of d_1, if we measure the characteristics of the width $2\bar{x}_0$ vs. the distance d_2 and find the temperature where the widths do not depend on the distance d_2, we can obtain the focal length $f(=d_1)$ vs. the temperature θ_0. Figure 13 shows the focal length vs. the temperature measured by the method mentioned above.

Now we compare the measured focal length to the theoretical one of [3]. We put the values of the constants, d (radius of the gas lens)$=0.85$ cm, l (length of the gas lens) $=45$ cm, T_0 (air input temperature)$=288°K$ into the equation of the focal length, obtained in [3]. We get the calculated value of the focal lengths, $1/f=0.10$ $(1/m)$ for $\theta_0=10°C$, 0.15 for $\theta_0=15°C$, and 0.20 for 20°C. We see that the agreement between calculated value and the measured is fair where the temperature θ_0 is low. From Fig. 13, we see that the reciprocal focal lengths are proportional to the temperature θ_0 in the range of the measurement.

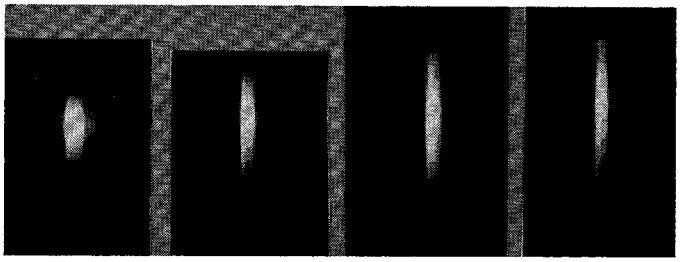

(a) $d_2=1$ m
(b) $d_2=2$ m
(c) $d_2=3$ m
(d) $d_2=4$ m

Fig. 8. Images of the line light source (LSF) formed by the gas lens when the distance d_2 is changed. The width of the slit (line light source) is 2 mm, the temperature θ_0 is 52°C, the wind velocity v is 0.31 m/s and the distance d_1 is 8.5 m.

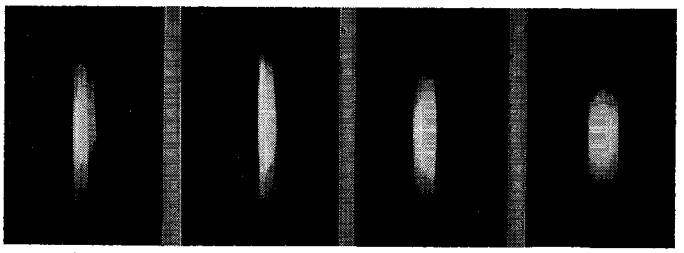

(a) $\theta_0=0$°C
(b) $\theta_0=17$°C
(c) $\theta_0=41$°C
(d) $\theta_0=74$°C

Fig. 9. Images of the line light source (LSF) formed by the gas lens when the temperature θ_0 is changed. The width of the slit is 1 mm, the wind velocity v is 0.32 m/s, and the distances are $d_1=8.65$ m, $d_2=4$ m.

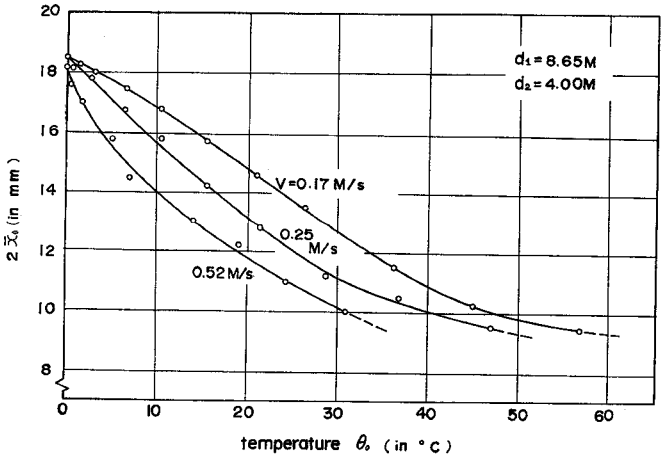

Fig. 10. Width $2\bar{x}_0$ of the line spread functions vs. the temperature with the wind velocity v as a parameter.

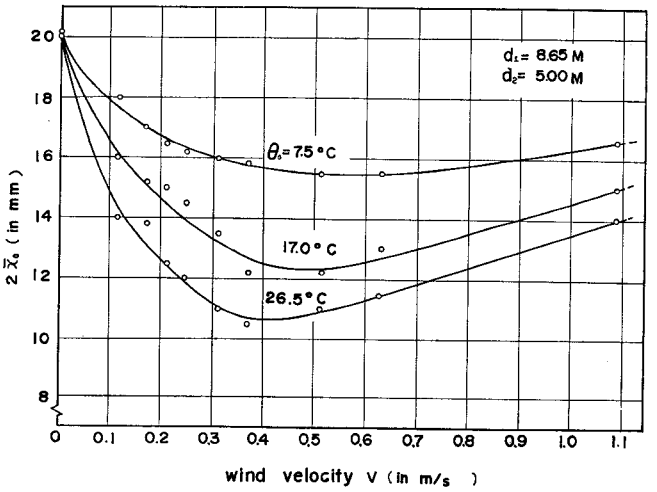

Fig. 11. Width $2\bar{x}_0$ of the line spread functions vs. the wind velocity v with the temperature θ_0 as a parameter.

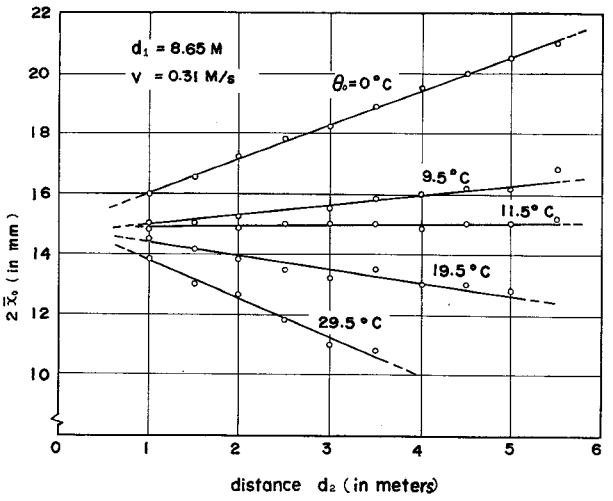

Fig. 12. Width $2\bar{x}_0$ of the line spread functions vs. the distance with the temperature θ_0 as a parameter.

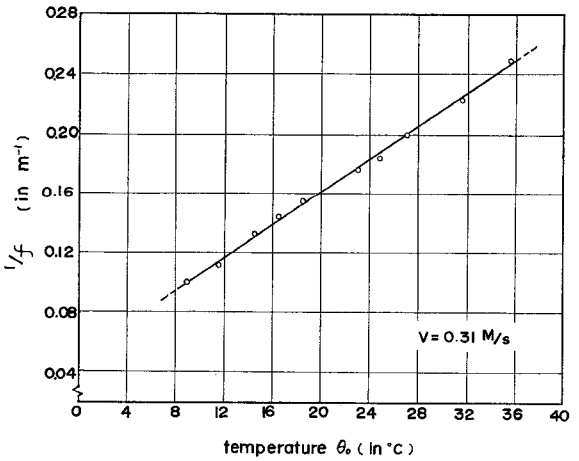

Fig. 13. Reciprocal focal length of the gas lens vs. temperature θ_0.

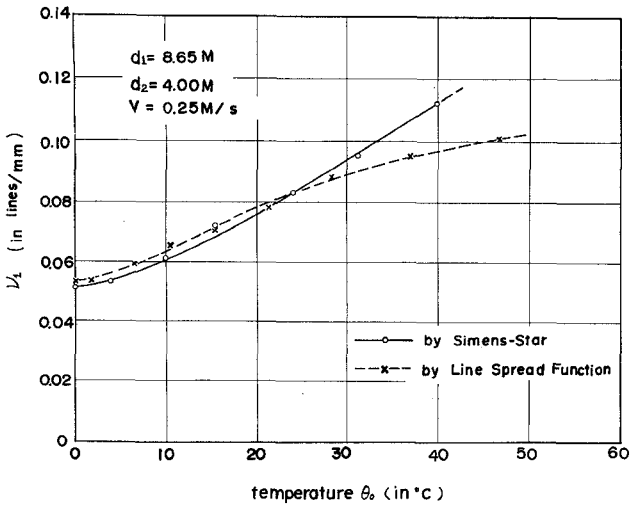

Fig. 14. Space frequencies ν_1 which give the first zero points of the optical transfer function of the gas lens vs. the temperature.

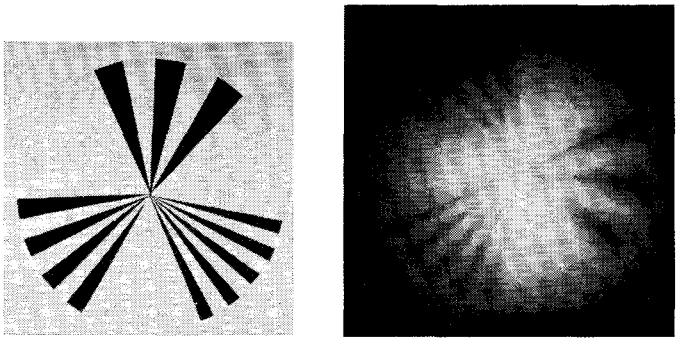

(a) (b)

Fig. 15. (a) Simens-star. (b) Image of the Simens-star. The temperature θ_0 is 25°C, the wind velocity v is 0.25 m/s and the distances are $d_1=8.5$ m, $d_2=4$ m.

VI. Optical Transfer Function of Gas Lens

The OTF gives the space-frequency bandwidth of a lens where the lens is considered as an optical spatial filter and the space frequencies which give the zero points of the OTF correspond, in a sense, to the cutoff frequencies of the filter. In the previous section it was considered that the LSF of the gas lens could be expressed by a rectangular function with a width of $2\bar{x}_0$ and we measure the widths vs. the variables (temperature, wind velocity, distance). Now that we know the width of the LSF, we can obtain the space frequencies which give the zero points of the OTF from (17). The dotted line of Fig. 14 shows the space frequencies ν_1 of the first zero points of the OTF vs. the temperature θ_0 which is obtained from the experimental results of Fig. 10.

The zero points of the OTF can also be obtained from the images of the Simens-star shown in Fig. 15(a). We construct the images of the Simens-star by the gas lens in the experimental arrangement as shown in Fig. 5, but with the slit replaced by the Simens-star. We then measure the distance L between two points of the arbitrary lines of the Simens-star where the inversion of the contrast of images begins to occur. Thus we can obtain the space frequency as $\nu_1=(1/L)$. Figure 15(b) shows the image of the Simens-star, where $d_1=8.5$ m, $d_2=4$ m, $v=0.25$ m/s, and $\theta_0=25$°C. We can recognize the inversion of the images though it is unclear.

The solid line of Fig. 14 shows the space frequencies obtained from the Simens-star. From Fig. 14 it is said that the space frequencies ν_1 obtained from the LSF do not show a large difference from the space frequencies ν_1 obtained from the images of the Simens-star. The maximum space frequencies of the zero points of the OTF appear when the image is in focus. For this reason, the OTF shown in Fig. 14 does not always have a maximum space-frequency bandwidth of the gas lens. However, the gas lens has a deep focus depth as mentioned in Section III and we roughly estimate the gas lens from the space-frequency bandwidth under the condition of Fig. 14. In Fig. 14 the bandwidth of the gas lens at the temperature $\theta_0=40$°C becomes about twice as great as the bandwidth at the temperature $\theta_0=0$°C where $d_1=8.65$ m, $d_2=4$ m and $v=0.25$ m/s. (The images at the temperature $\theta_0=0$°C caused by the pin hole effect, were mentioned in Section III.) However, the space frequency of the gas lens under the conditions as mentioned above ($\theta_0=40$°C) is about 0.1 line/mm and this is much narrower than that of an ordinary glass lens. Therefore, to use the gas lens as an optical lens, the improvements of the gas lens are required from various points, such as types of gas lens, optimum control of the refractive index gradients, stability of images, species of gases, temperature, gas velocity, gas pressure, and so forth.

VII. Telescope Using Gas Lens

In the preceding section we investigated the imaging properties of the gas lens and found that the gas lens acted as a convex lens. Here we describe the construction of an optical system using a gas lens. Figure 16 shows a Keplerian telescope arrangement using a gas lens for an object lens and a concave mirror for an eye lens.

The gas lens used in this experiment is 960 mm in length with a diameter of 13 mm. A concave mirror of a reflecting telescope with a focal length of 840 mm is used as an eye lens. Figure 17 shows scenery taken by an ordinary camera and Fig. 18(a) is a distant view of the framed part of Fig. 17 as seen by the telescope using the gas lens, where the distance d_2 between the gas lens and the concave mirror is 3.8 m, the temperature θ_0 is 16.5°C, and the wind velocity v is 1.35 m/s. Figure 18(b) is a photograph taken when the action of the gas lens is stopped. This results in an image of poor quality due to the pin hole effect stated in Section III. From Fig. 18, it is evident that the gas lens acts as an object lens and a telescopic effect is produced. However, as far as brightness is concerned, the images of the telescope using the gas lens are darker than those of a reflection telescope. Clear views are seen when the distance d_2 is changed from about 3 meters to about 12 meters while the field of view becomes narrower as the distance d_2 increases. This fact may be explained from the experimental results stated in Section III in which the images of the gas lens become larger as the distance d_2 between the gas lens and image plane increases.

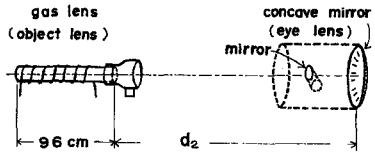

Fig. 16. Keplerian telescope with a gas lens for an object lens and a concave mirror for an eye lens.

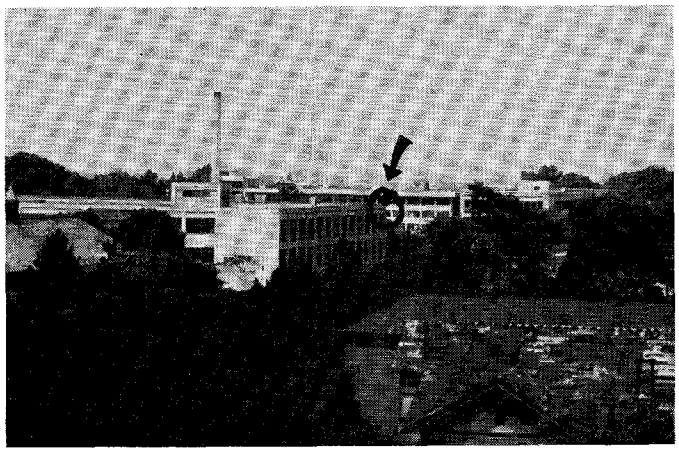

Fig. 17. Scenery taken by an ordinary camera.

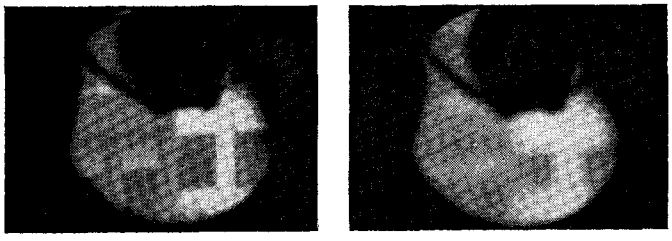

(a) (b)

Fig. 18. (a) The circled part of Fig. 17 seen by the Keplerian telescope shown in Fig. 16. (b) Photograph taken when the action of the gas lens was stopped.

VIII. Conclusion

Theoretical and experimental analyses on the imaging properties of gas lens were performed. The lens effects were examined experimentally by changing the variable parameters (temperature, gas velocity, distance) that are concerned with the imaging action of the gas lens.

As a result of the experiment, it was ascertained that the gas lens used in this experiment acted like a convex lens with a large focal length and a deep focus depth coupled with pin hole effect coming from the small diameter of the metal pipe. A gas lens is a parameter-variable lens unlike a single glass lens. That is to say, the parameters of a lens (focal length, curvature, refractive index, etc.) can be varied by controlling the temperature gradients, gas velocity, gas pressure, and so forth. This is one point where the gas lens is applicable to some optical systems. Further, we can obtain a lens of a large focal length without the trouble of polishing the glass, though it is necessary to control the refractive index of gas. The large focal length of a gas lens is applicable to telescopic systems and a Keplerian telescope was made using a gas lens for an object lens. A fairly good telescope was produced. The problems of optimum design of gas lenses, controlling the refractive index, stability of the images, aberrations, etc., are dependent on future studies of gas lenses.

Acknowledgment

The authors wish to thank Assistant Prof. A. Nishitsuji and the staff of the Research Institute of Applied Electricity at the Hokkaido University for their cooperation in this work. They are also indebted to Y. Kinoshita and Y. Fujiwara, graduate students of the Department of Electronic Engineering for discussions and help in the experiments, and to all those who freely gave their advice in this work.

References

[1] D. W. Berreman, "A lens or light guide using convectively distorted thermal gradients in gases," *Bell Sys. Tech. J.*, vol. 43, p. 1469, July 1964.
[2] ——, "A lens using unlike counter-flowing gases," *Bell Sys. Tech. J.*, vol. 43, p. 1476, July 1964.
[3] D. Marcuse and S. E. Miller, "Analysis of a tubular gas lens," *Bell Sys. Tech. J.*, vol. 43, p. 1759, July 1964.
[4] A. C. Beck, "Thermal gas lens measurements," *Bell Sys. Tech. J.*, vol. 43, p. 1818, July 1964.
[5] ——, "Gas mixture lens measurements," *Bell Sys. Tech. J.*, vol. 43, p. 1821, July 1964.
[6] E. A. J. Marcatili, "Mode in a sequence of thick astigmatic lens-like focusers," *Bell Sys. Tech. J.*, vol. 43, p. 2887, November 1964.
[7] P. K. Tien, J. P. Gordon, and J. R. Whinnery, "Focusing of a light beam of Gaussian field distribution in continuous and periodic lens-like media," *Proc. IEEE*, vol. 53, p. 455, February 1965.
[8] H. Kogelnik, "Imaging of optical modes-resonators with internal lenses," *Bell Sys. Tech. J.*, vol. 44, p. 455, March 1965.
[9] Y. Suematsu and H. Fukinuki, "Analysis of the idealized light waveguide using gas lens," *J. IECE (Japan)*, vol. 48, p. 1684, October 1965.
[10] D. Marcuse, "Theory of a thermal gradient gas lens," *IEEE Trans. on Microwave Theory and Techniques*, vol. MTT-13, p. 734, November 1965.
[11] W. H. Steier, "Measurements on a thermal gradient gas lens, *IEEE Trans. on Microwave Theory and Techniques*, vol. MTT-13, p. 740, November 1965.
[12] Y. Aoki and M. Suzuki, "Imaging action of gas lens," *Oyo Buturi*, vol. 35, p. 193, March 1966.
[13] H. Kubota, *Oyo Kogaku*. Tokyo, Japan: Iwanami Book Co., 1959, p. 204.
[14] E. L. O'Neill, *Introduction to Statistical Optics*. London: Addison-Wesley, 1963, p. 12.
[15] M. Born and E. Wolf, *Principles of Optics*. New York: Pergamon, 1964, p. 110.
[16] M. Suzuki and Y. Aoki, "Theoretical consideration of gas lens," *Bulletin of the Faculty of Technology, Hokkaido University*, vol. 38, p. 90, August 1965.
[17] Y. Aoki, "Light rays in lens-like media," to be published in *J. Opt. Soc. Am.*
[18] T. Inoue, K. Ogawa, and M. Iwanaga, "Image analysis of thermal neutron radiograph," *Oyo Buturi*, vol. 34, p. 801, November 1965.